COMMUNICATION

Room-Temperature Tunneling Behavior of Boron Nitride Nanotubes Functionalized with Gold Quantum Dots

*Chee Huei Lee, Shengyong Qin, Madhusudan A. Savaikar, Jiesheng Wang, Boyi Hao, Dongyan Zhang, Douglas Banyai, John A. Jaszczak, Kendal W. Clark, Juan-Carlos Idrobo, An-Ping Li, and Yoke Khin Yap**

Boron nitride nanotubes (BNNTs)[1,2] and boron nitride nanosheets (BNNSs)[3] have gained increasing attention for their structural similarity to carbon nanotubes (CNTs) and graphene, respectively. These BN nanostructures are wide-bandgap materials (~6 eV), and their electronic properties are different from those of CNTs and graphene. In addition, BNNTs and BNNSs offer intriguing properties that are not available in carbon nanostructures. For example, the bandgap of BNNTs is not sensitive to the change of their diameters, chiralities, and number of tubular shells. Furthermore, their bandgap is tunable by doping, the giant Stark effect, and structural deformation.[1,2] However, due to their electrically insulating nature, BNNTs and BNNSs cannot be used as conduction channels in electronic devices and sensors. Doping of BNNTs with carbon[4] and fluorine[5] has led to phase segregation and defective BNNTs, respectively. Obviously doping has failed to convert BNNTs into semiconductors. More recently, bent BNNTs have been shown to conduct a minute current,[6,7] which is attributed to their radial deformation that was predicted to result in a reduced bandgap. The insulating nature of BNNTs and BNNSs prevents them from being used as conduction channels in electronic devices.

On the other hand, semiconductors, such as Si, are indispensable for electronic devices including field-effect transistors (FETs). However, future FETs will encounter various fundamental limitations,[8,9] including i) high power consumption due to leakage in the semiconducting channels; ii) short channel effects as the conduction length approaches the scale of the depletion layer width, and iii) high contact resistance at the semiconducting channels. Novel device concepts have been proposed to overcome these issues including the exploration of alternative gating architecture,[10] tunneling FETs (TFETs)[11] and spintronic devices.[9] In particular, TFETs with a low turn-on voltage and high sub-threshold slope are important for next-generation very-large-scale integration (VLSI) technology. All these devices are still based on semiconductors.

Here, we show a novel method by using BNNTs to create room-temperature TFETs without using semiconductors. Our devices are based on quantum tunneling between gold quantum dots deposited on the insulating BNNTs (QDs-BNNTs). We show that QDs-BNNTs are insulating at low bias voltages, but allow electron tunneling only when sufficient potential is applied. Since the switching behavior is based on quantum tunneling, these TFETs have suppressed leakage current and contact resistance. In addition, the performance of our TFETs is enhanced at a shorter tunneling channel, in contrast to the short channel effects in Si devices. Thus, QDs-BNNTs are advanced materials for TFETs that could bypass some of the fundamental limitations in semiconducting channels.

High-quality BNNTs can be grown by the growth-vapor-trapping (GVT) approach.[12] The as-grown BNNTs are insulators with diameters of ~20–80 nm. These BNNTs are used as one-dimensional (1D) channel substrates for the deposition of gold QDs by pulsed-laser deposition (PLD).[13] BNNTs are almost ideal as the substrates for the deposition of these QDs due to their uniform and controllable diameters. Furthermore, their ideally defect-free sp^2 BN network makes them chemically inert to the deposited QDs, and remains electrically insulating. **Figures 1**a and 1b show the microscopic images of as-prepared QDs-BNNTs under scanning electron microscopy (SEM) and scanning transmission electron microscopy (STEM).[14] The gold QDs are crystalline (Figure 1c) and are preferentially deposited on one side of the BNNTs. Due to the spatial confinement of the BNNT channel substrate, these QDs form a one-dimensional (1D) array of particles with estimated diameters that range from about 3–10 nm and an inter-dot spacing of about 1–5 nm (see Figure S1 in the Supporting Information). As shown in the SEM images, the morphology and structural properties of BNNTs remained unchanged after QD coating. Characteristic signals collected by Raman spectroscopy (Figure 1d) and Fourier transformed IR spectroscopy (Figure 1e) are nearly identical to those of as-grown BNNTs.[12]

As-deposited QDs-BNNTs are then electrostatically transferred to oxidized Si substrates by mechanical rubbing (see Figure S2 in the Supporting Information). The transferred QDs-BNNTs are well dispersed and aligned horizontally. We characterize the electronic properties of these QDs-BNNTs at room temperatures by using a four-probe scanning tunneling microscopy

Dr. C. H. Lee, M. A. Savaikar, Dr. J. S. Wang, B. Y. Hao, Dr. D. Y. Zhang, D. Banyai, Prof. J. A. Jaszczak, Prof. Y. K. Yap
Department of Physics
Michigan Technological University
Houghton, MI 49931, USA
E-mail: ykyap@mtu.edu
Dr. S. Y. Qin, Dr. K. W. Clark, Dr. A.-P. Li
Center for Nanophase Materials Sciences
Oak Ridge National Laboratory
Oak Ridge, TN 37831-6487, USA
Dr. J.-C. Idrobo
Materials Science and Technology Division Oak Ridge National Laboratory, Oak Ridge, TN 37831-6487, USA

DOI: 10.1002/adma.201301339

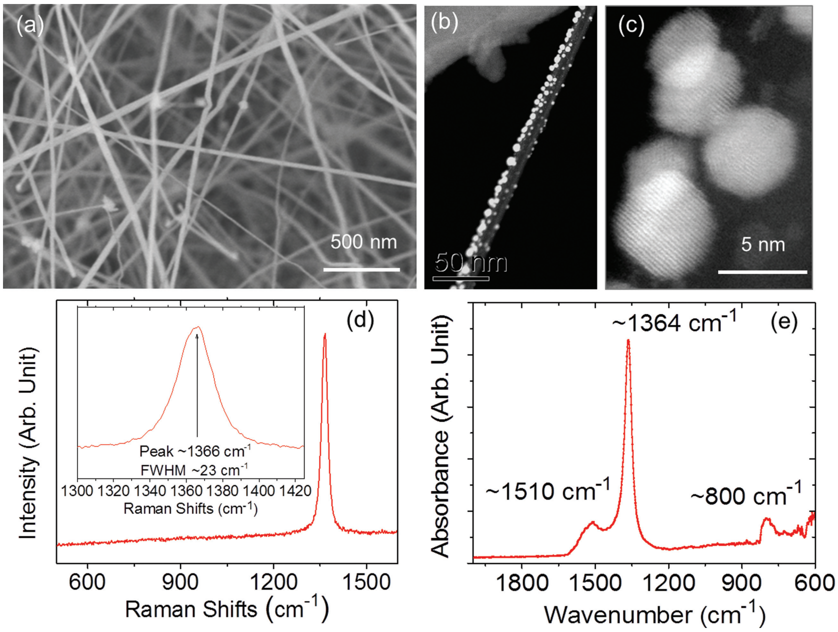

Figure 1. Microscopic images of QDs-BNNTs obtained by (a) scanning electron microscopy (SEM) and (b,c) scanning transmission electron microscopy (STEM). (d) Raman and (e) Fourier-transform IR spectra obtained from QDs-BNNTs.

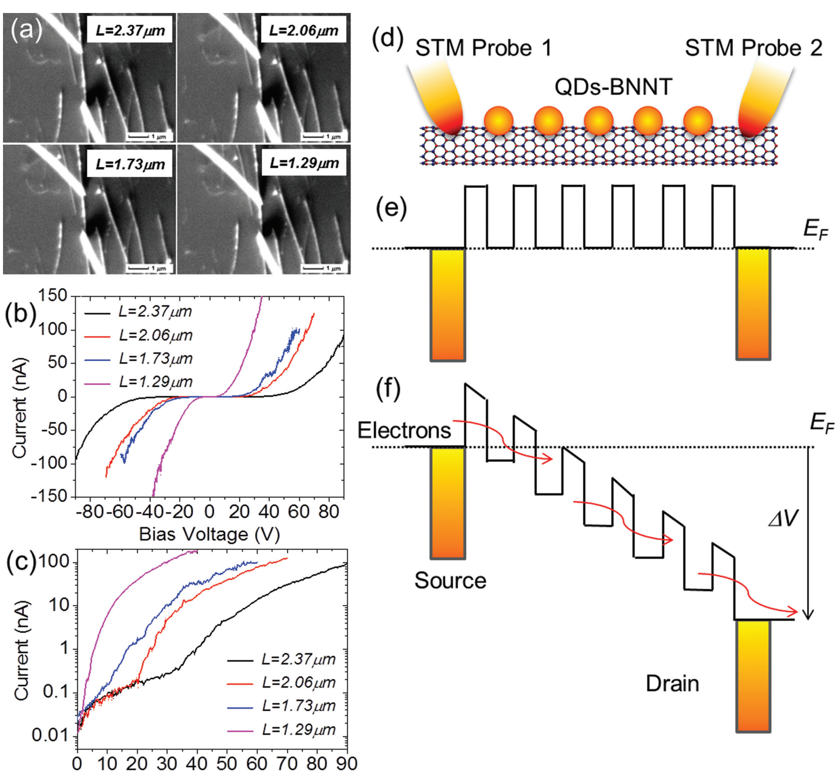

Figure 2. (a) SEM images of a QD-BNNT nanostructure as contacted by two STM probes at various conduction channel lengths (L) and the corresponding *I–V* characters measured at room temperature (b,c). (d) Schematic of a QDs-BNNT in contact with two STP probes and the corresponding energy diagram (e). (f) Electron tunneling across the QDs due the applied electric field between the probes.

(4-probe STM) system.[15] **Figure 2**a shows an isolated QDs-BNNT in contact with two STM probes at a desired channel length (*L*). This QD-BNNT nanostructure is as insulating as pure BNNTs ("off" state, current ~10^{-11} A) at low bias voltages (Figure 2b and 2c). At higher bias voltages, the QDs-BNNT can switch to a conducting state ("on" state) with a current level as high as ~10^{-7} A. Current–voltage (*I–V*) curves in Figure 2c show that the turn-on voltages (V_{on}) of QD-BNNT decrease from about 34.0 to 2.0 V as the nanotube length *L* decreases from 2.37 to 1.29 μm. Based on the current levels of the "on" and the "off" states, the on-off ratio is estimated to be on the order of 10^4.

We show that the observed behavior is consistent with the Coulomb blockade behavior. As shown in Figures 2d and 2e, potential barriers are present between the gold QDs, as they are physically isolated from each other. The capacitances of the QDs are sufficiently small (10^{-19}–10^{-18} F) such that the charging energies ($E_c \sim e^2/C$) for tunneling are appreciable (E_c ~ 100 meV) in these systems.[16] Here, e is the magnitude of electron charge and C is the total capacitance of a particular QD. By applying an electric potential (V_{sd}) across the QDs with the STM probes acting as source and drain electrodes, a potential gradient is established across the QD array, as illustrated schematically in Figure 2f. This leads to a series of potential drops (V_{ij}) across neighboring pairs of islands i and j. Experimentally these V_{ij} are non-uniform, and the capacitances vary along the array due to variations in QD size and spacing. Electron tunneling occurs only when a sufficient V_{ij} develops between a pair of QDs such that the free energy ($-eV_{ij} + E_{c,ij}$) decreases in the transition. $E_{c,ij}$ is defined as the junction charging energy, which depends solely upon the capacitances of the system (See Supporting Information). Before V_{sd} is large enough to maintain a steady state of tunneling transitions, current flow is prohibited by the Coulomb blockade in the device. As V_{sd} increases, there is also an accompanying band bending between QDs, as illustrated in Figure 2f. In the "on" state, the *I–V* characteristics depend on the nature of the tunneling process across the junctions. In addition, we note that since the geometric shapes of the QDs are irregular, we expect the presence of sharp points that could enhance the local electric fields between these QDs, therefore facilitating the tunneling processes.

Based on this hypothesis, a theoretical model is developed to simulate these

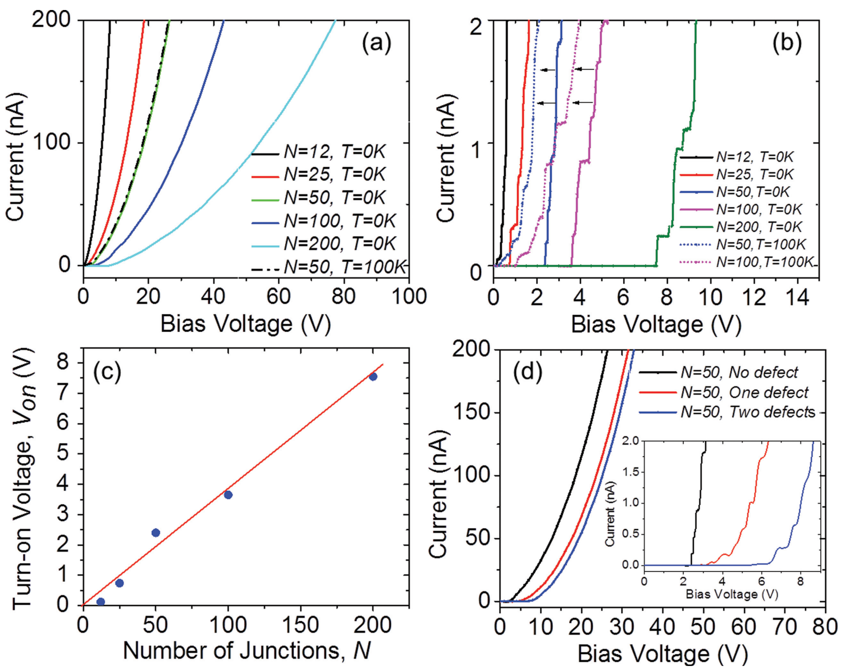

Figure 3. (a,b) Calculated *I*–*V* curves of QDs-BNNTs with various numbers of gaps (N) at T = 0 K. L for N = 12, 25, 50, 100, and 200 correspond to 0.11, 0.24, 0.48, 0.96, and 1.92 µm, respectively. *I*–*V* curves for N = 50 and N = 100 at T = 100 K are also shown for comparison. (c) Turn-on voltage (V_{on}) as a function of the number of junctions (N) along the conduction channel. (d) *I*–*V* curves for N = 50 with zero, one, and two defects (gap distances are ~8–10 nm) at T = 0 K.

switching behaviors based on semi-classical theory[16] and kinetic Monte Carlo simulation methods[17] (see Supporting Information). **Figures 3**a and 3b show the simulated *I*–*V* behavior of QD-BNNTs at temperatures T = 0 and 100 K, and with various number of junctions, N (i.e., the number of gaps between QDs, which is proportional to the conduction length, L). As shown in Figure 3b, V_{on} increases with N and the trend is consistent with our experimental observations (Figure 2b). In addition, the effect of temperature is not obvious at the full current scale and large biases (cases for N = 50 in Figure 3a). This is also confirmed experimentally where the *I*–*V* characteristic are nearly identical for T = 82 and 250 K (see Figure S4 in the Supporting Information). Theoretically, Coulomb staircases are observed at the low bias and low current regimes (Figure 3b) where the work done on an electron crossing a junction, eV_{ij}, is comparable to the junction charging energy from the tunneling electron, $E_{c,ij}$. Because these differences in energy are small, thermal effects are more pronounced in this regime. As shown in Figure 3b, V_{on} at T = 100 K (dotted curves) is lower than V_{on} at T = 0 K and the Coulomb staircases are less pronounced. These are due to the increase in thermal energy (k_BT, where k_B is the Boltzmann constant, T is the temperature in Kelvin), which effectively reduces width of the Coulomb blockade. The *I*–*V* characteristics at T = 100 K for N = 50 and 100 (dotted curves in Figure 3b) show that the effective blockade width is sensitive to temperature. With increasing temperature, blockade effects are smeared and a sharp increase in current at V_{on} is smoothed out, and thus V_{on} decreases. Higher-temperature *I*–*V* curves shift towards the lower bias values with the Coulomb staircases shifting towards lower current values. However, this temperature-dependent current change is too small to be detected experimentally with our setup.

As shown in Figures 3a and 3b, V_{on} for shorter conduction channels (smaller N) is lower than those of longer channels. The result indicates that V_{on} can be reduced by having a shorter conduction length or fewer QDs (Figure 3c). This is an attractive feature of QD-BNNTs as one may reduce the feature size of devices towards zero-dimensional (0D) with short QD-BNNTs for lower operational power consumption. This result suggests that QD-BNNTs are prospective materials for room-temperature 0D switches in the future.

There is strong qualitative agreement between the *I*–*V* characteristics of the simulated and experimental devices as discussed so far. However, the theoretical V_{on} values are lower than the experimental ones. This is because our simulation is conducted for an ideal 1D array of QDs. In the actual conditions, the QDs are not perfectly aligned (pseudo-1D) with the direction of the applied electric field, which leads to reduction of the local field between QDs. Furthermore, distances between some QDs can be larger (up to ~10 nm) than the average values (1–5 nm) (see Figure S1 in the Supporting Information). Additional simulations were conducted to investigate the effect of these defects. To model a defect in the QD array, simulations were conducted on arrays with one or a pair of QDs removed at random from the ideal N = 50 array already studied. As shown in Figure 3d, V_{on} increases significantly with the presence of defects as well as the number of defects.

Finally, the effect of gate potential was also investigated experimentally. Since the detected tunneling current is due to the band bending and potential drops across the QD junctions, it is expected that the transition energies through the $E_{c,ij}$ term could be modulated by a gate potential and thus their *I*–*V* characteristics could be changed. In view of this, we have examined the transport properties across QD-BNNTs by applying a gate potential on the Si substrate (back-gate configuration). As shown in **Figures 4**a and 4b, the switching behaviors of a QD-BNNT, namely V_{on} values, can be modified by gate voltages, with a tunable range between zero and 4.8 V at L = 1.42 µm. We note that the measured *I*–*V* characteristics appear to be symmetrical under positive and negative biasing; however, they are actually slightly asymmetrical. The symmetry is due to the overall relative uniformity of the QD distribution (less defective), which leads to a relatively uniform distribution of capacitances along the chain. Shorter chain-length devices and devices with asymmetrically distributed larger defects (variances in island size or spacings), would be expected to show increased asymmetry in the *IV* characteristics. We also noted that recent work with regular QD diameters and inter-dot spacing in a series of SiO_2 nanotrenches did not lead to room temperature switching. This

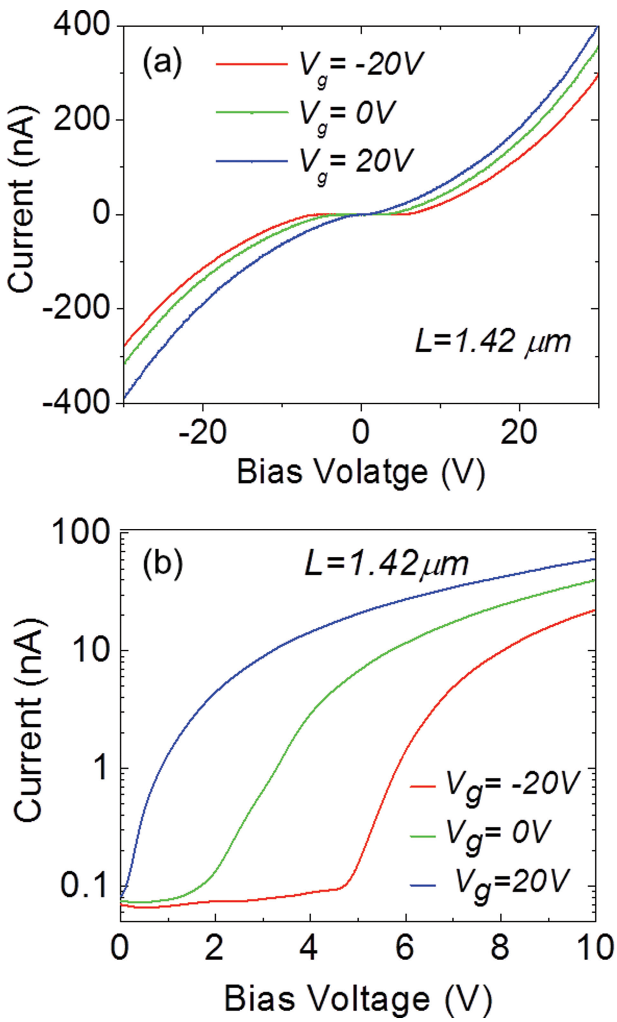

Figure 4. (a) Transport properties of a QDs-BNNT at room temperature under the modulation of gate voltages (V_g). (b) Transport properties near the thresholds.

may signify that the QD structural irregularity and larger inter-dot spacing demonstrated here by QD-BNNTs play an important role for room-temperature switching.[18] The on-off ratio for a single channel of a QD-BNNT is also two orders of magnitude larger than that measured for 160 channels of QDs assembled in the nanotrenches.

In summary, we have demonstrated a new paradigm of electronic switches at room temperature without using semiconducting channels. Creative use of metallic QDs on a 1D insulator (BNNTs) has led to a new class of room-temperature tunneling switches. We show that V_{on} can be reduced by using a shorter conduction length and varying the gate potential. Theoretically, these tunneling channels can be miniaturized into 0D. Furthermore, the diameters of the QDs and the inter-dot spacing can be irregular, signifying the defect-tolerant nature of these tunneling channels. More research is required to further understand and improve the transport properties of these QD-BNNTs by preparing QDs with uniform and controllable diameters and inter-dot spacing.

Experimental Section

Depostion of QDs on BNNTs by PLD: Deposition of gold quantum dots (QDs) on BNNTs was conducted by using the fourth harmonic generation (wavelength = 266 nm, pulse duration = 5 ns) of a Nd:YAG laser and a gold (Au, 99.99%) target (1" in diameter). An as-grown BNNT sample was placed on the PLD substrate holder (facing the gold target) and sealed inside the vacuum chamber at a base vacuum as high as ~5×10^{-7} mbar (10^{-9} Torr). Deposition of gold QDs was conducted at room temperature in vacuum with a pulsed UV laser energy of about 10 mJ. The deposition was ended when a film thickness of 6 nm was recorded by the quartz monitor. Arrays of Au QDs are self-assembled on BNNTs at room temperature and are referred to as QD-BNNTs.

Scanning transmission electron microscopy: STEM imaging and spectroscopy analysis were performed on an aberration-corrected Nion UltraSTEM-100 operating at 60 kV. The convergence semi-angle for the incident probe was 31 mrad. ADF images were collected for a half-angle range of ~86–200 mrad.

Transport properties measurement: The as-transferred QD-BNNTs on oxidized Si substrates were mounted on a sample stage of the 4-probe STM system, where gate potential can be applied in a back gate configuration. After identifying a well-dispersed QDs-BNNT under SEM, two tungsten probes were directly contacted on two ends of the nanotube with desired distances (conduction length, *L*). Potential differences were then applied across the two probes to characterize the transport properties of QD-BNNTs.

Supporting Information

Supporting Information is available from the Wiley Online Library or from the author.

Acknowledgements

This work is supported by the U.S. Department of Energy, the Office of Basic Energy Sciences (Grant DE-FG02-06ER46294, PI:Y.K.Y.). Theoretical simulation was performed in part using the computing cluster wigner.research.mtu.edu in Information Technology Services and rama.phy.mtu.edu in the Department of Physyics at Michigan Technological University. Part of this work was conducted at the Center for Nanophase Materials Sciences (Projects CNMS2009-213 and CNMS2012-083, PI:Y.K.Y.), which is sponsored at Oak Ridge National Laboratory (ORNL) by the Scientific User Facilities Division, Office of Basic Energy Sciences, U.S. Department of Energy (DOE), and by ORNL's Shared Research Equipment (ShaRE) User Program (JCI), which is sponsored by the Office of Basic Energy Sciences, U.S. DOE.

Received: March 25, 2013
Revised: May 15, 2013
Published online: June 17, 2013

[1] a) D. Golberg, Y. Bando, C. C. Tang, C. Y. Zhi, *Adv. Mater.* **2007**, *19*, 262; b) D. Golberg, Y. Bando, Y. Huang, T. Terao, M. Mitome, C. C. Tang, C. Y. Zhi, *ACS Nano* **2012**, *4*, 2979; c) J. S. Wang, C. H. Lee, Y. K. Yap, *Nanoscale* **2010**, *2*, 2028; d) J. S. Wang, C. H. Lee, Y. Bando, D. Golberg, Y. K. Yap, in *B-C-N Nanotubes and Related Nanostructures*, (Ed: Y. K. Yap), Springer, **2009**, Ch. 2.
[2] a) A. Rubio, J. L. Corkill, M. L. Cohen, *Phys. Rev. B* **1994**, *49*, 5081–5084; b) N. G. Chopra, R. J. Luyken, K. Cherrey, V. H. Crespi, M. L. Cohen, S. G. Louie, A. Zettl, *Science* **1995**, *259*, 966.
[3] L. Song, L. Ci, H. Lu, P. B. Sorokin, C. Jin, J. Ni, A. G. Kvashnin, D. G. Kvashnin, J. Lou, B. I. Yakobson, P. M. Ajayan, *Nano Lett.* **2010**, *10*, 3209.

[4] K. Suenaga, C. Colliex, N. Demoncy, A. Loiseau, H. Pascard, F. Willaime, *Science* **1997**, *278*, 653.
[5] C. Tang, Y. Bando, Y. Huang, S. Yue, C. Gu, F. Xu, D. Golberg, *J. Am. Chem. Soc.* **2005**, *127*, 6552.
[6] X. Bai, D. Golberg, Y. Bando, C. Zhi, C. Tang, M. Mitome, K. Kurashima, *Nano Lett.* **2007**, *7*, 632.
[7] H. M. Ghassemi, C. H. Lee, Y. K. Yap, R. S. Yassar, *Nanotechnology* **2012**, *23*, 105702.
[8] a) T. N. Theis, P. M. Solomon, *Science* **2010**, *327*, 1600; b) M. Lundstrom, *Science* **2003**, *299*, 210.
[9] J. J. L. Morton, D. R. McCamey, M. A. Eriksson, S. A. Lyon, *Nature* **2011**, *479*, 345.
[10] I. Ferain, C. A. Colinge, J. P. Colinge, *Nature* **2011**, *479*, 310.
[11] A. M. Ionescu, H. Riel, *Nature* **2011**, *479*, 329.
[12] a) C. H. Lee, M. Xie, V. K. Kayastha, J. S. Wang, Y. K. Yap, *Chem. Mater.* **2010**, *22*, 1782; b) C. H. Lee, J. S. Wang, V. K. Kayatsha, J. Y. Huang, Y. K. Yap, *Nanotechnology* **2008**, *19*, 455605.
[13] J. S. Wang, V. K. Kayastha, Y. K. Yap, Z. Y. Fan, J. G. Lu, Z. W. Pan, I. N. Ivanov, A. A. Puretzky, D. B. Geohegan, *Nano Lett.* **2005**, *5*, 2528.
[14] W. Zhou, J. Lee, J. Nanda, S. T. Pantelides, S. J. Pennycook, J.-C. Idrobo, *Nat. Nanotechnol.* **2012**, *7*, 161.
[15] T. H. Kim, X. G. Zhang, D. M. Nicholson, B. M. Evans, N. S. Kulkarni, B. Radhakrishnan, E. A. Kenik, A. P. Li, *Nano Lett.* **2010**, *10*, 3096.
[16] D. V. Averin, K. K. Likharev, in *Mesoscopic Phenomena in Solids*, (Eds: B. L. Altshuler, P. A. Lee, R. A. Webb), Elsevier **1991**, Ch. 6.
[17] A. B. Bortz, M. H. Kalos, J. L. Lebowitz, *J. Comput. Phys.* **1975**, *17*, 10.
[18] K. Xu, L. D. Qin, J. R. Heath, *Nat. Nanotechnol.* **2009**, *4*, 368.

ADVANCED MATERIALS

Supporting Information

for *Adv. Mater.*, DOI: 10.1002/adma.201301339

Room-Temperature Tunneling Behavior of Boron Nitride Nanotubes Functionalized with Gold Quantum Dots

*Chee Huei Lee, Shengyong Qin, Madhusudan A. Savaikar, Jiesheng Wang, Boyi Hao, Dongyan Zhang, Douglas Banyai, John A. Jaszczak, Kendal W. Clark, Juan-Carlos Idrobo, An-Ping Li, and Yoke Khin Yap**

DOI: 10.1002/adma.201301339

Room Temperature Tunneling Behaviors of Boron Nitride Nanotubes Functionalized with Gold Quantum Dots

By *Chee Huei Lee, Shengyong Qin, Madhusudan A. Savaikar, Jiesheng Wang, Boyi Hao, Dongyan Zhang, Douglas Banyai, John A. Jaszczak, Kendal W. Clark, Juan-Carlos Idrobo, An-Ping Li, Yoke Khin Yap****

Dr. C. H. Lee, M. A. Savaikar, Dr. J. S. Wang, B. Y. Hao, Dr. D. Y. Zhang, D. Banyai, Prof. John A. Jaszczak, Prof. Y. K. Yap
Department of Physics
Michigan Technological University
Houghton, MI 49931, USA.
E-mail: ykyap@mtu.edu

Dr. S. Y. Qin, Dr. K. W. Clark, Dr. A. P. Li
Center for Nanophase Materials Sciences
Oak Ridge National Laboratory
Oak Ridge, TN 37831-6487, USA.

Dr. J. C. Idrobo
Materials Science and Technology Division
Oak Ridge National Laboratory
Oak Ridge, TN 37831-6487, USA.

Keywords: Boron nitride, nanotubes, quantum dots, tunneling, field effect transistors

Supporting Information

1. One-dimensional QD array on BNNTs

As estimated by the contrast line profile extracted from a Scanning transmission electron microscopy (STEM) image of a QDs-BNNT (Figure S1), these QDs have an average diameter ranging from about 3-10 nm with gap spacing of about 2-5 nm in between. As shown in Figure S1, larger gaps (~10nm) are occasionally detected.

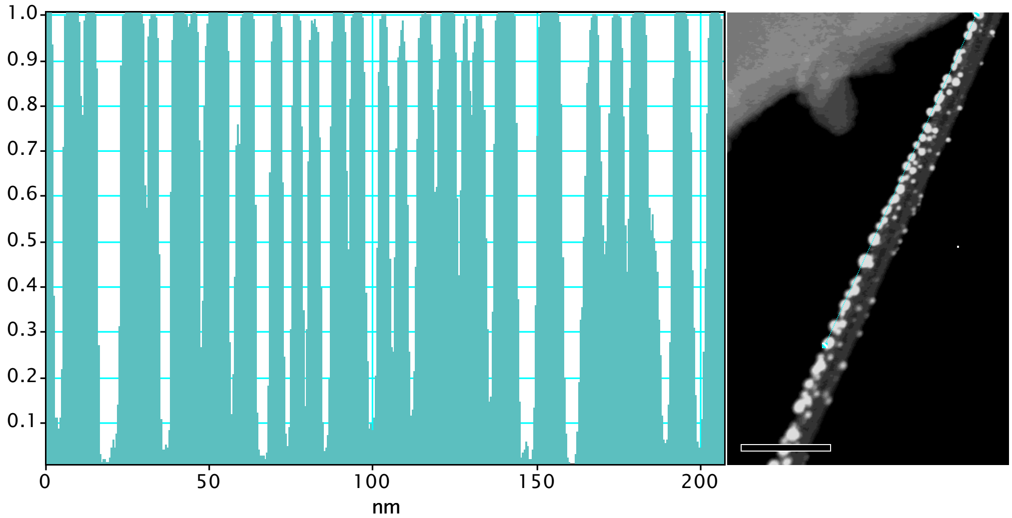

Figure S1. Normalized contrast line profile (left) across the array of gold QDs scanned along the green line (upper right to lower left) indicated in the STEM image (right).

2. Electrostatic transfer of QDs-BNNTs by mechanical rubbing

As-deposited QDs-BNNTs can be transferred to clean oxidized Si substrates by mechanical rubbing. This approach allows for the clean transfer of QDs-BNNTs with good dispersion without involving suspension and dispersion of the nanotubes in any liquid media. This was performed by placing the as-deposited QDs-BNNTs on a clean oxidized Si surfaces (with 500 nm thermal oxide). The QDs-BNNT sample was then pressed down lightly (equivalent to a 50-100g load) and then dragged along the surface of the clean substrate as shown in Figure S2. The as-transferred QDs-BNNTs are aligned along the rubbing direction as shown in the SEM images. The density/dispersion level depends on the initial density of the as-grown BNNT sample and can be controlled by the rubbing rate and the pressing forces.

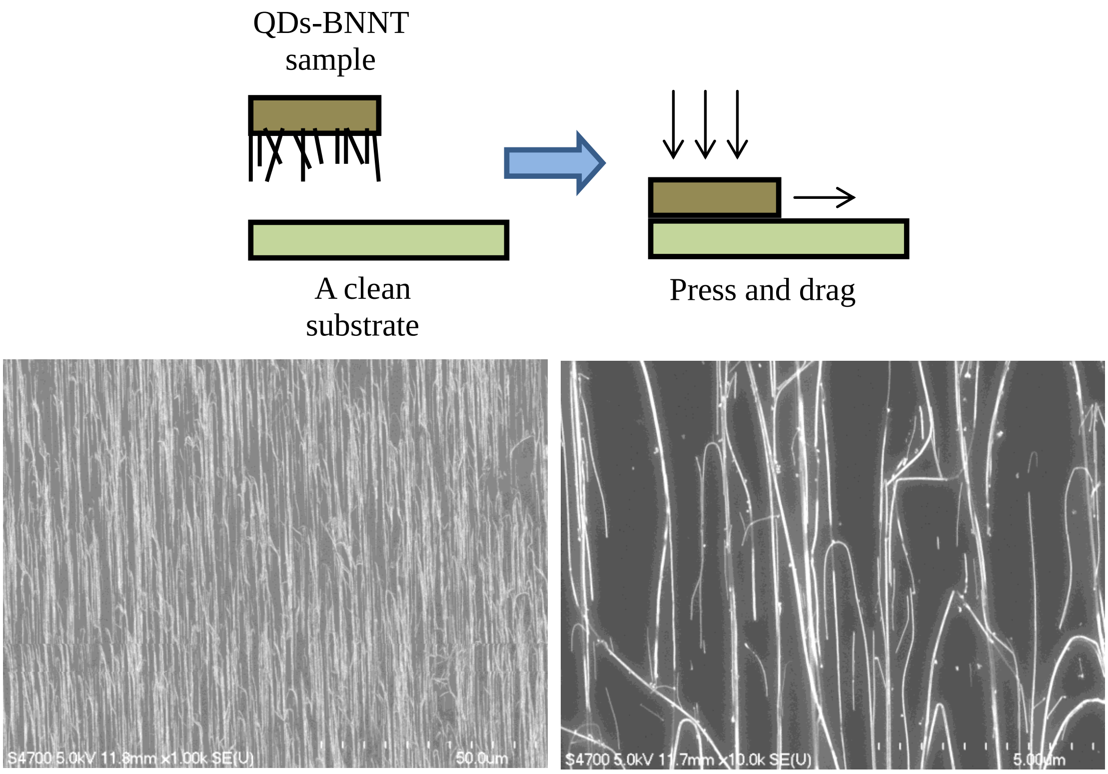

Figure S2. Procedure of electrostatic transfer of QDs-BNNTs on a clean oxidized Si substrate (top). Scanning electron microscopy (SEM) images of as-transferred nanotubes with well alignment and dispersion.

3. Characterization by four-probe scanning tunneling microscopy (4-probe STM)

All QDs-BNNTs were characterized at room temperature (unless otherwise noted) using a 4-probe STM system under ultrahigh vacuum (base pressure $<2\times10^{10}$ Torr)).[1] Figure S3 shows the typical leakage current of the sample at various gate potential (in the order of 10^{-11}A). This leakage current is a few orders or magnitude lower than the detected current across QDs-BNNTs discussed in the manuscript.

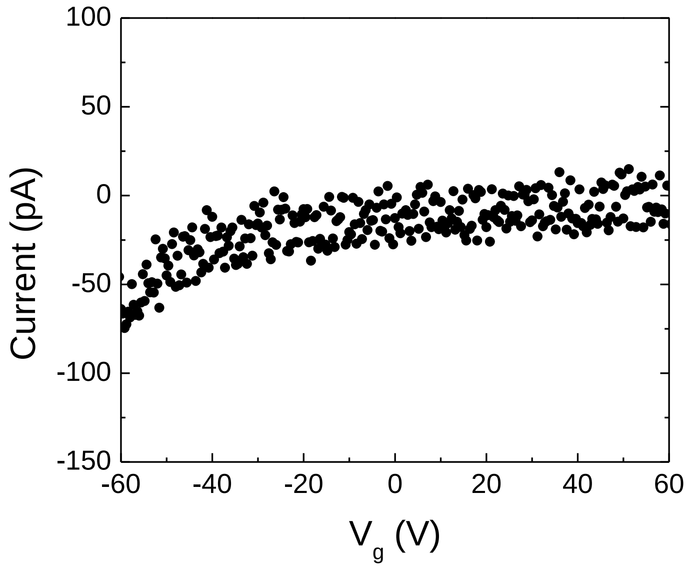

Figure S3. Leakage current at various gate voltages (V_g) detected from a typical QDs-BNNT sample.

4. Theoretical Simulation

The QDs-BNNT system is modeled by a one-dimensional chain of 200 spherical conductors (QDs), with nearest neighbors separated by an insulating tunnel junction (gap between QDs). The radius of each QD is randomly selected between 3 and 10 nm, while the junction widths randomly vary between 1 nm and 5 nm. A fixed QD at the end of the chain is selected as the drain electrode at a bias voltage *V*, while the source (ground) electrode is chosen from among the remaining QDs in the chain according to the desired number of QDs in the system.

For a given voltage across the source and drain electrodes, the current through the device is computed using kinetic Monte Carlo simulation methods [2, 3] based on computed electron tunneling rates across the junctions. For the calculation of the tunneling rates we follow a semi-classical approach (orthodox theory), which assumes that (i) the energy spectrum of the conductive QDs may be considered continuous, i.e. $\Delta E << k_B T$, (ii) the tunneling time is negligible compared to the time between tunneling events, and (iii) coherent tunneling events are ignored. [4, 5] Thus, for a pair of QDs *i* and *j*, the tunneling rate is given by [6, 7]

$$\Gamma_{ij}(\Delta W_{ij}) = \left(\frac{\Delta W_{ij}}{e^2 R_{ij}}\right)\left[1 - \exp\left(-\frac{\Delta W_{ij}}{k_B T}\right)\right]^{-1},$$

where R_{ij} is the tunneling resistance of the junction, T is the temperature, e is the electron charge, k_B is the Boltzmann constant, and ΔW_{ij} is the change in the electrostatic energy of the system due to the tunneling event (see below).

The tunneling resistance plays a key role in determining the tunneling rate for a junction, as it depends exponentially on the separation d_{ij} between QDs and on the work function of the QD ϕ, as well as other system parameters like the Fermi energy E_F and the QD radii. Values of E_F and ϕ approximate for gold were chosen as 5.5 eV and 4.8 eV, respectively. If the potential difference between two QDs is significant compared to the work function, the height of the tunneling barrier should be taken to decrease linearly from one QD to the next; however, to simplify the calculations, the tunneling barrier is taken to be of constant height across the width of the junction, but with a reduced height that varies with the potential drop across the junction according to $\phi_{eff} = \phi - V_{ij}/2$. Thus the tunneling resistance is given by [8]

$$R_{ij} = \left(\frac{h^3}{64\pi^2 m_e e^2}\right)\left(\frac{E_F + \phi_{eff}}{E_F}\right)^2 \frac{\exp(2\alpha k_0 d_{ij})}{\phi_{eff}}\left(\frac{\alpha k_0}{r_a}\right)\frac{1}{G_{ij}},$$

where $k_0 = (2\pi/h)(2m_e\phi_{eff})^{1/2}$, and h is the Planck constant. m_e is the free electron mass, and α is an enhancement factor (= 0.115) for the fitting of the overall current scale. G_{ij} is a purely geometrical factor that takes into account the solid angle subtended by one spherical QD at the other across the tunnel junction when considering the current flux, and is given by

$$G_{ij} = 1 - \left(1 - \left\{ r_a \big/ (r_a + d_{ij}) \right\}^2\right)^{1/2},$$

where r_a is the average radius of the two spherical QDs forming the junction, and d_{ij} is the closest distance between their surfaces (the junction width).

The change in free energy due to the transition is given by, $\Delta W_{ij} = eV_{ij} - E_{c,ij}$ which depends on V_{ij}, the potential drop across the junction, and $E_{c,ij}$, the charging energy for the transition as determined by capacitances of the system. [4, 6, 9] An analytical method employing image charges was used for the calculation of junction capacitances C_{ij} between neighboring QDs. [10, 11] The junction capacitances are given by

$$C_{ij} = 4\pi\varepsilon\varepsilon_0 \frac{r_i r_j}{d_{c,ij}} (\sinh x)\sum_{n=1}^{\infty}(\sinh nx)^{-1}, \text{ where } x \equiv \cosh^{-1}\left[\frac{d_{c,ij}^2 - (r_i^2 + r_j^2)}{2r_i r_j}\right],$$

r_i and r_j are the radii of the respective QDs forming the junction, and $d_{c,ij}$ is the center-center distance between them. The number of image charges n required for good convergence consistent with the boundary conditions depends on the ratio of junction width to the radius of the spheres (*d/r*). For our system, 100-125 image charges were found to be sufficient for good convergence. In addition to the junction capacitances, the charging energy also depends on the self capacitances of the QDs (between the QD and ground). The self-capacitance of QD *i* is given by $C^i_{self} = 4\pi\varepsilon\varepsilon_0 r_i$, where ε is the dielectric constant (taken as 1 here) and ε_0 is the vacuum permittivity.

For a given system of a chain of QDs between fixed source and drain electrodes, the resistances and capacitances are computed, from which the tunneling rates for all the junctions are determined. A tunneling event is selected based on kinetic Monte Carlo methods, and the charge and potential distribution in the system is updated. The process is repeated for large number of cycles until the current through the device reaches a steady state and the current is computed to satisfactory statistical precision.

Theoretical current-voltage (*I-V*) characters of QDs-BNNTs at T = 0 K and 100 K are discussed in the main text. These *I-V* curves are identical at the large current scale. This result suggests that such simulation is sufficient to explain the experimental *I-V* properties detected at room temperature. This is also proven experimentally, where *I-V* characters of a QDs-BNNT at T = 82 K (L=0.53 μm) and 250 K (L=0.38 μm) are nearly identical as shown in Figure S4. Note that these measurements are performed on the same section of the same QDs-BNNT with a slight change in the conduction lengths (L) during the change of the temperature setting.

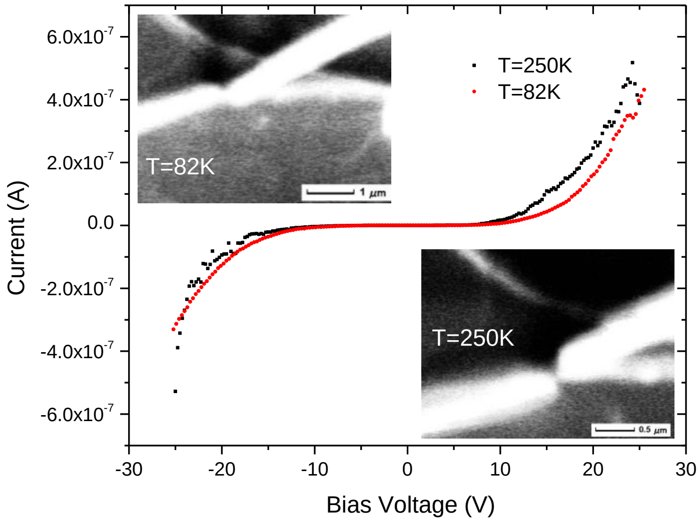

Figure S4. *I*-*V* characters of a QDs-BNNT at T = 82 K (*L*=0.53 μm) and 250 K (*L*=0.38 μm) as measured at the same section on the same QDs-BNNT.

References

[1] T. H. Kim, X. G. Zhang, D. M. Nicholson, B. M. Evans, N. S. Kulkarni, B. Radhakrishnan, E. A. Kenik, A. P. Li, *Nano Letters* **2010**, *10*, 3096.

[2] A. B. Bortz, M. H. Kalos, J. L. Lebowitz, *J. Comput. Phys.* **1975**, *17*, 10.

[3] M. Kotrla, *Comput. Phys. Commun.* **1996**, *97*, 82.

[4] K. K. Likharev, *Proc. IEEE* **1999**, *87*, 606.

[5] C. Wasshuber, *Computational Single-Electronics*, Springer **2001**.

[6] D.V. Averin and K.K. Likharev, in *Mesoscopic Phenomena in Solids*, (Eds: B. L. Altshuler, P. A. Lee, R. A. Webb), Elsevier **1991**, Ch. 6.

[7] M. Amman, R. Wilkins, E. Benjacob, P. D. Maker, R. C. Jaklevic, *Phys Rev B* **1991**, *43*, 1146.

[8] A. S. Cordan, A. Goltzene, Y. Herve, M. Mejias, C. Vieu, H. Launois, *J. Appl. Phys.* **1998**, *84*, 3756.

[9] M. Amman, M, R. Wilkins, E. Ben-Jacob, P. D. Maker, R. C. Jakevic, *Phys. Rev. B* **1991**, *43*, 1146.

[10] E. Pisler, T. Adhikari, *Physica Scripta* **1970**, *2*, 81.

[11] J. Lekner, *J. Electrostat* **2011**, *69*, 11.